



CHORUS

This is the accepted manuscript made available via CHORUS. The article has been published as:

## Influences of Exciton Diffusion and Exciton-Exciton Annihilation on Photon Emission Statistics of Carbon Nanotubes

Xuedan Ma, Oleskiy Roslyak, Juan G. Duque, Xiaoying Pang, Stephen K. Doorn, Andrei Piryatinski, David H. Dunlap, and Han Htoon

Phys. Rev. Lett. **115**, 017401 — Published 2 July 2015

DOI: [10.1103/PhysRevLett.115.017401](https://doi.org/10.1103/PhysRevLett.115.017401)

# Influences of Exciton Diffusion and Exciton-Exciton Annihilation on Photon Emission Statistics of Carbon Nanotubes

Xuedan Ma<sup>1†</sup>, Oleskiy Roslyak<sup>1,5</sup>, Juan G. Duque<sup>2</sup>, Xiaoying Pang<sup>3</sup>, Stephen K. Doorn<sup>1</sup>, Andrei Piryatinski<sup>4\*</sup>, David H. Dunlap<sup>6\*</sup>, and Han Htoon<sup>1\*</sup>

<sup>1</sup>Center for Integrated Nanotechnologies, Materials Physics and Applications Division, <sup>2</sup>Physical Chemistry and Applied Spectroscopy, Chemistry Division, <sup>3</sup>High Power Electrodynamics, Accelerator Operations and Technology Division, <sup>4</sup>Theoretical Division, Los Alamos National Laboratory, Los Alamos, New Mexico, 87545, USA. <sup>5</sup>Department of Physics and Engineering Physics, Fordham University, Bronx, New York, 10458, USA. <sup>6</sup>Department of Physics and Astronomy, University of New Mexico, Albuquerque, New Mexico, 87131, USA.

## Abstract

Pump-dependent photoluminescence imaging and 2<sup>nd</sup> order photon correlation studies have been performed on individual single-walled carbon nanotubes (SWCNTs) at room temperature that enable the extraction of both the exciton diffusion constant and the Auger recombination coefficient. A linear correlation between these is attributed to the effect of environmental disorder in setting the exciton mean free-path and capture-limited Auger recombination at this lengthscale. A suppression of photon antibunching is attributed to creation of multiple spatially non-overlapping excitons in SWCNTs whose diffusion length is shorter than the laser spot size. We conclude that complete antibunching at room temperature requires an enhancement of the exciton-exciton annihilation rate that may become realizable in SWCNTs allowing for strong exciton localization.

Nonclassical photon emission statistics (photon-antibunching) of single quantum emitters such as single atoms [1], molecules [2], quantum dots [3], and nitrogen-vacancy centers in diamond [4] have been recently investigated intensively for development of single photon sources needed for realization of quantum communication . These studies have been extended to single-walled carbon nanotubes (SWCNTs) [5-7], which are near-perfect one-dimensional (1d) semiconductors allowing for fast exciton migration [8-10]. Provided the lowest energy band is populated by more than one exciton, one cannot expect strong photon antibunching from such 1d systems. Studies have revealed that antibunching is possible at cryogenic temperatures due to strong localization of excitons and their subsequent exciton-exciton annihilation (EEA) [5-7], yet so far no systematic studies have been conducted at room temperature on photon statistics of delocalized, 1d excitons. While diffusion, on one hand, facilitates antibunching by allowing for EEA of spatially separated excitons, it could, on the other hand, lead to spreading of the exciton population leading to independent emission of multiple photons. In this Letter, we systematically examine the interplay of these two processes on SWCNT photon emission statistics. This could shed a new light on the feasibility of SWCNT based room-temperature single photon sources.

Exciton diffusion and EEA have been the focii of many previous studies because they play critical roles in defining photoluminescence (PL) characteristics of SWCNTs. Evidence of EEA has been observed in the form of pump-dependent variations in PL decay dynamics [11-13] as well as saturation behaviors of PL [14,15] and transient absorption signals [20]. Many attempts have also been made to determine the exciton diffusion length,  $L_D$ , in SWCNTs [8,16-19], revealing values ranging from nanometers [9] to hundreds of nanometers [10,16,19]. The large discrepancies in these measurements have been attributed to effects of pump power [10], differences in fabrication methods (CoMoCAT or HiPco) [8,10], and the environment

(surfactant- or DNA-wrapped or air-suspended) [8,10] of the SWCNTs. Among these factors, the pump-dependence of  $L_D$  arises from an increase of the EEA rate with the square of the exciton population, a consequence of bi-molecular processes [20]. Yet, in spite of the well developed Smolochowski-Noyes theory for reaction diffusion processes [21], the EEA term has not been fully incorporated into the 1d diffusion equation in analysis of the pump dependence of the PL intensity profiles [10]. Our study below reveals that EEA processes in SWCNTs have multiple lengthscale contributions associated with both  $L_D$  and the exciton mean free-path,  $\xi$ .

To address these open issues, we performed pump power-dependent PL imaging and 2<sup>nd</sup> order photon correlation ( $g^{(2)}$ ) studies on individual (6, 5) SWCNTs. We spread deoxycholate (DOC) wrapped, chirality sorted [22,23] HiPco [24] SWCNTs on glass substrates with density less than one nanotube per  $100 \mu\text{m}^2$  area. A standard micro-PL system (see Supplementary section S1 for details) was used to perform single SWCNT PL imaging and  $g^{(2)}$  experiments. Predominantly (6, 5) SWCNTs with lengths distributed in 1.2 to 2.6  $\mu\text{m}$  range were excited at their  $E_{22}$  resonance of 570 nm with femtosecond laser pulses. We first imaged each SWCNT by illuminating them entirely using a wide-field mode and subsequently determined their lengths from the FWHM of their axial PL intensity profiles (Fig. 1a and 1g). Then we confocally excited the SWCNTs at their centers with a laser spot having a diameter  $\sigma_0 = 455 \text{ nm}$ . Resulting pump-dependent PL images of two SWCNTs with the lengths of 1.2 and 2.6  $\mu\text{m}$  (Figs. 1b-1e and 1h-1k) show PL profiles broadening along their lengths, indicating spreading of the exciton population beyond the extent of the laser spot. For the 1.2  $\mu\text{m}$  SWCNTs (Fig. 1b-1e), the FWHM of the axial PL intensity profile increases with the rise of pump fluence and saturates at very high pump fluences (Fig. 1f). In contrast, in the case of the longer 2.6  $\mu\text{m}$  SWCNTs (Fig. 1h-1k), the profile shrinks with the increase of the pump fluence (Fig. 1i). Data validating our analysis on PL

profiles and more examples of pump dependent PL intensity profiles supporting these trends are given in S2-S4 and S5, respectively.

This interesting pump dependence cannot be explained in terms of a linear 1d diffusion equation and requires an explicit nonlinear term describing the EEA processes [10]. Here, we treat EEA as an exciton coalescence reaction (i.e.,  $A + A \rightarrow A$ ) [25]. For the problem of interest this process is governed by the following equation for the exciton density,  $n(x, t)$ ,

$$\frac{\partial n(x, t)}{\partial t} = -k_{1X}n(x, t) + D\frac{\partial^2 n(x, t)}{\partial x^2} - C_{EEA}(t)n^2(x, t). \quad (1)$$

Here,  $k_{1X}$  is the exciton decay rate determining the PL lifetime in the absence of EEA,

$D = L_D^2 k_{1X}$  is the exciton diffusion constant, and

$$C_{EEA}(t) = C_A \left( 1 - \frac{1 - \sqrt{2\varepsilon} \operatorname{erf}[\sqrt{2\varepsilon\alpha t}] - e^{\alpha(1-2\varepsilon)} \operatorname{erfc}[\sqrt{\alpha t}]}{1 - 2\varepsilon} \right) \quad (2)$$

is a time-dependent EEA coefficient (dimensionality  $nm / ps$ ) where the prefactor  $C_A$  is the Auger recombination coefficient corresponding to the microscopic electron-hole recombination processes at the lengthscale of the exciton mean free-path,  $\xi$ . In the Smoluchowski-Noyes theory of diffusion-limited reactions leading to Eq. (1), the diffusion of two particles in their center of mass frame is equivalent to the diffusion of a single particle in the presence of a reaction (i.e., recombination) center with twice the diffusion constant. The first term in the parentheses of Eq. (2) (i.e., unity) arises specifically in 1d since a particle in the neighborhood of a reaction center has a high probability of immediately finding it. The second term describes the formation of a depletion region in the vicinity of a reaction center at a rate  $\alpha = C_A^2 / 4D$ , and  $(\operatorname{erfc}[x]) \operatorname{erf}[x]$  denotes the (complementary) error function. In S6, we demonstrate that Eq. (2) is a generalization of the constant Auger rate model previously used to interpret EEA signatures observed in

ultrafast decay of PL PL [12,26] and transient absorption [12,27] signals, and PL saturation behavior [14,15]. The model interpolates between a constant  $C_{EEA} = C_A$  valid at short times, to the time-dependent  $C_{EEA}(t) \sim t^{-1/2}$  at long-times used in Refs. [9,28] to interpret the EEA dynamics as 1d diffusion-limited recombination. In addition, this accounts for the limitations on the EEA imposed by the exciton decay process via the dimensionless ratio  $\varepsilon = 2k_{1X} / \alpha$  comparing the rate of exciton decay to the rate of depletion region formation.

The goal of the PL data analysis is to attain a single set of diffusion lengths,  $L_D = \sqrt{D/k_{1X}}$  ( $k_{1X} = 1/55 \text{ ps}^{-1}$  for DOC-wrapped SWCNTs [16]) and Auger coefficients,  $C_A$ , fitting *all* the intensity profiles *for each tube* measured at *different* excitation powers. For this purpose a fitting procedure described in S7 and based on Eqs. (1) and (2) is used. In contrast to prior studies [13, 21, 24] where single intensity profiles were fit to extract  $L_D$ , we have simultaneously fit 4 to 9 intensity profiles composed of 80 to 180 data points [25] and extracted a *single* set of  $L_D$  and  $C_A$  for each SWCNT. Fig. 1f and 1i display examples of the best-fit curves along with the experimental data points providing  $L_D = 289 \text{ nm}$ ,  $C_A = 382 \text{ nm}^2/\text{ps}$  and  $L_D = 718 \text{ nm}$ ,  $C_A = 447 \text{ nm}^2/\text{ps}$ , respectively. Notice that in Figs. 1f the inset represents a general trend for the widths,  $\sigma$ , of *all* measured PL profiles to *broaden* with the increasing pump power provided SWCNTs have  $L_D < \sigma_0$ . In contrast, inset in Fig. 1i shows that SWCNTs having  $L_D > \sigma_0$  demonstrate *narrowing* of the PL profile with increasing pump power. Numerical simulations discussed in S8 and based on Eqs. (1) and (2) clearly reproduce these trends.

To rationalize the trends, we estimate average PL profile widths as  $\sigma^2 = \sigma_0^2 + \Delta\sigma^2$ , where  $\Delta\sigma^2 = 2D\tau_{EEA}$  describes the contribution of exciton diffusion to the profile spread on the EEA

timescale  $\tau_{EEA} \approx \frac{D\sigma_0}{(N_0 - 1)C_A^2}$ . Here,  $N_0$  is the number of excitons prepared by the pulse that can

be evaluated from absorption cross section of SWCNT ( $\bar{\sigma} = 10^{-12} \text{ cm}^2/\mu\text{m}$ ) as shown in S7.

[29,30] This timescale is estimated by solving Eq. (1) describing EEA at short times by setting

$k_{1x} = 0$  as described in S6. Thus,  $\Delta\sigma^2 \sim 1/N_0$  indicating that the PL profiles should narrow if

the number of excitons (pump power) increases. Since the natural upper limit on  $\Delta\sigma$  is  $L_D$ , one

can expect this trend to be observed for the initial profile widths  $\sigma_0 < L_D$ . This is exactly the case

in Fig. 11. In the opposite case ( $\sigma_0 > L_D$ ) the diffusive contributions to the PL profiles become

negligible. The EEA processes occur predominately in the center of the Gaussian pulse where the exciton concentration is the highest. This reduces the amount of PL intensity relative to the

radiation of the Gaussian tails, effectively leading to a spatial broadening of the integrated

radiation profile, (Fig. 1f inset). In the same wide-profile limit, it should also be noted that two

excitons initially separated by a distance  $\gtrsim L_D$  never interact over the course of the experiment

and effectively belong to different segments of a SWCNT and can be considered to be

independent emitters. An exciton density prepared within the laser spot of width  $\sigma_0 \gg L_D$  can be

split into  $m \approx \sigma_0 / L_D$  independent emitters.

Fig. 2 presents values of  $C_A$  vs  $D = L_D^2 k_{1x}$  obtained from a global fit of the PL intensity profiles of 26 SWCNTs, yielding diffusion constants in the range of  $D \sim 6 \times 10^2 - 4.4 \times 10^3 \text{ nm}^2/\text{ps}$  ( $L_D \sim 182 - 492 \text{ nm}$ ). This is in good agreement with the results of recent measurements [8,16]. At the same time, our analysis yields Auger coefficients in the range  $C_A \sim 200 - 750 \text{ nm/ps}$ . Although  $C_A$  and  $D$  vary for each SWCNT, we find a strong *linear* correlation between them.

To rationalize the correlation between  $C_A$  and  $D$ , we recall that the exciton energy landscape in SWCNTs is perturbed by environmentally induced disorder[16]. This limits exciton coherent motion characterized by mean velocity,  $v$ , to a mean free-path,  $\xi$ , giving rise to a diffusion constant  $D = v\xi$ . By taking into account that  $v = \sqrt{k_B T / m^*}$ , where  $k_B T$  is thermal energy and the ratio of exciton effective mass to electron mass in vacuum is  $m^* / m_0 \sim 0.05$ , we use experimental values in Fig. 2, to estimate the variation range of mean free-path to be  $\xi \sim 4 - 15$  nm. We further assume that two-excitons form a *bound state* with a delocalization length *less* than  $\xi$  before experiencing Auger recombination. As demonstrated in S9, in contrast to direct Auger recombination [31], such a *capture-limited* Auger process can be described by the Auger constant being proportional to  $\xi$ . Specifically,  $C_A = \xi / 2\tau_{2X,A}$ , where,  $\tau_{2X,A}$  is native Auger recombination time of the bound two-exciton complex. Therefore, observed variation in the values of  $D$  and  $C_A$  reflects an environment-induced variation of  $\xi$  in the ensemble of SWCNTs. By taking the ratio of  $D$  to  $C_A$  we find the experimentally observed linear correlation whose slope value gives  $\tau_{2X,A} = 10$  fs (see S9). Furthermore, capture-limited Auger recombination requires formation of a bound two-exciton state on the timescale less than  $\tau_{2X,A}$ . The analysis in S9 suggests that such an ultrafast exciton capture might be facilitated by Coulomb mediated long-range exciton-exciton interactions.

Crossover between single and multiple independent quantum emitter regimes in SWCNTs has clear signatures in photon emission statistics. The quantity of interest is the degree of photon-antibunching  $R_0$  at the low pump fluence limit available from the measurements of 2<sup>nd</sup> order photon correlation function,  $g^{(2)}$ . For a *single* quantum emitter in the small spot size limit

( $\sigma_0 < L_D$ ),  $R_0 = Q_{2X} / Q_{1X}$  where  $Q_{2X}$ , and  $Q_{1X}$  are two-exciton-to-exciton and exciton quantum yields, respectively. [32,33] In the limit of large spot size ( $\sigma_0 > L_D$ ), the *minimum* attainable degree of photon-antibunching is  $R_0 = (m - 1) / m$ . Here,  $m = \sigma_0 / (cL_D)$  is the number of independent emitters each of size  $cL_D$  where a scaling parameter  $c \sim 1 - 2$  is introduced to facilitate fitting of the experimental data. We use a generalized expression for  $R_0$  accounting for  $m$  (including  $m = 1$ ) independent emitters and two exciton emission/recombination processes given by [34]

$$R_0 = \frac{p_2 Q_{2X}}{m Q_{1X}} + \frac{m - 1}{m}. \quad (3)$$

Here,  $p_2 = 2P_2^{(N)} / (P_1^{(N)})^2$  is the ratio of Poisson probabilities to produce two and one excitons, respectively, and  $\langle N \rangle$  is the average number of absorbed photons.[35]

To examine the significance of the two terms in Eq. (3), we performed pump-dependent  $g^{(2)}$  measurements on 15 SWCNTs and analyzed  $R_0$  in terms of the ratio  $\sigma_0 / L_D \sim m$  for fixed  $\sigma_0 = 455$  nm, using values of  $L_D$  obtained from the analysis of PL intensity profiles. Figs. 3a-3c display representative pump-dependent  $g^{(2)}$  traces of 3 SWCNTs with the shortest, medium, and the longest values of  $L_D$  having  $\sigma_0 / L_D = 2.5, 1.4$ , and  $0.8$ . In Fig. 3d,  $R_0$  is plotted as a function of pump fluence expressed in terms of the average number of absorbed photons per pulse,  $\langle N \rangle$  (see S7). The data clearly show that the  $R_0$  values gradually increase with  $\langle N \rangle$  for all SWCNTs. This trend is more pronounced for the medium- $L_D$  SWCNTs (Fig. 3d) showing the smallest the smallest value of  $R_0 = 0.4$  (Fig. 3b, bottom trace) at the lowest pump fluence. However, for the

longest and shortest diffusion length SWCNTs (bottom traces in Fig. 3a and 3c), we observe  $R_0 > 0.6$ .

The  $R_0$  values vs.  $\sigma_0 / L_D$  measured from all 15 SWCNTs are plotted in Fig. 4. This plot shows that while minimum values of  $0.4 \leq R_0 \leq 0.5$  are observed in SWCNTs with  $L_D / \sigma_0 = 1.0 - 1.7$ ,  $R_0$  increases for both smaller and larger values of  $\sigma_0 / L_D$ . To interpret the observed trends, we have evaluated  $R_0$  using Eq. (3) along with an independent quantum emitter model (see S10) parameterized by the values of  $L_D$  and  $C_A$  attained from the analysis of the PL intensity profiles. Calculated total  $R_0$  and contributions due to each term in Eq. (3) are shown in Fig. 4. A best fit is obtained by setting the size of each independent emitter to  $cL_D = 1.6L_D$  and the prefactor  $p_2 = 1.5$  corresponding to  $\langle N \rangle = 0.4$  (consistent with Fig. 3c). For  $\sigma_0 / L_D \gtrsim 1.6$  ( $m \gtrsim 1$ ), the calculation shows excellent agreement with experiment and is dominated by the multiple emitter term  $(m-1)/m$ . As the diffusion length approaches the laser spot size ( $\sigma_0 / L_D \sim 1.2 - 1.6$ ), the contribution of  $(m-1)/m$  decreases toward zero approaching the single quantum emitter regime ( $m \sim 1$ ) in which the ratio  $Q_{2X} / Q_{1X}$  fully determines  $R_0$ . Constant behavior of  $R_0$  at this length scale is due to the weak dependence of the EEA rate on  $L_D$  illustrated in S10.[36] For  $\sigma_0 / L_D < 1$ , the calculation of  $R_0$  does not reproduce the experimental trend, revealing the limitation of the coarse-grained estimate of  $Q_{2X}$  (see S10).

Observed limitations for  $R \gtrsim 0.4$  seem to contradict experimental reports of strong antibunching found in SWCNT low temperature PL emission [5-7]. However, at cryogenic temperatures, potential fluctuations along the length of the SWCNT become deep enough to trap the excitons. These traps become recombination centers for all the excitons created within  $L_D$  and

yield highly localized PL emission regardless of  $L_D$ . Since the exciton trapping strongly enhances the efficiency of the EEA process, PL emission of a single trap site exhibits near complete antibunching. This type of localization-induced antibunching cannot be observed for band-edge excitons at room temperature due to large thermal fluctuations. However, it may become possible in oxygen doped SWCNTs that emit from a deep trap level located 160 meV below the band edge exciton [37].

In conclusion, the pump-dependent PL intensity profiles measured from individual SWCNTs have been examined. An analysis based on the Smolochowski-Noyes reaction-diffusion equation with a time-dependent EEA coefficient reveals a linear correlation between  $C_A$  and  $D$  that is attributed to the effect of environmental disorder in setting the exciton mean free-path whose values are estimated to vary in the range of  $\xi \sim 4 - 15$  nm. Linear dependence of the Auger coefficient on mean free-path,  $C_A \sim \xi$ , further suggests ultrafast capture-limited Auger recombination of exciton pairs. Both pump-dependence of PL profile widths and 2<sup>nd</sup> order photon correlation measurements confirm creation of multiple spatially non-overlapping excitons forming independent emitters in SWCNTs whose diffusion length is shorter than the laser spot size, i.e.,  $\sigma_0 \gtrsim L_D$ . The 2<sup>nd</sup> order photon correlation measurements provide a value of  $1.6L_D$  for the size of an independent quantum emitter, and clearly show a drop in the minimal degree of photon antibunching to  $R_0 \sim 0.5$  as the number of independent emitters approaches unity. Further reduction of  $R_0$  requires significant decrease in the two-exciton-to-exciton quantum yield,  $Q_{2X}$ . This can be achieved at room temperature via an enhancement of the EEA rate and may become realizable in SWCNTs with strong exciton localization. These findings have pertinence for the development of SWCNT-based room-temperature single photon sources, and the analysis may be applied to other 1d nanomaterials such as conjugated polymers and semiconductor nanowires.

This work was conducted, in part, at the Center for Integrated Nanotechnologies (CINT), a U.S. Department of Energy, Office of Basic Energy Sciences (OBES) user facility and supported in part by Los Alamos National Laboratory Directed Research and Development Funds.

\*Corresponding authors:

AP: [apiryat@lanl.gov](mailto:apiryat@lanl.gov)

DHD: [dunalp@unm.edu](mailto:dunalp@unm.edu)

HH: [hhtoon@lanl.gov](mailto:hhtoon@lanl.gov)

†Present address: Center for Integrated Nanotechnologies, Sandia National Laboratories, Albuquerque, New Mexico 87185, USA

## References:

- [1] H. J. Kimble, M. Dagenais, and L. Mandel, *Phys. Rev. Lett.* **39**, 691 (1977).
- [2] T. Basche, Moerner, W. E., Orrit, M. & Talon, H., *Phys. Rev. Lett.* **69**, 1516 (1992).
- [3] P. Michler, A. Imamoglu, M. D. Mason, P. J. Carson, G. F. Strouse, and S. K. Buratto, *Nature* **406**, 968 (2000).
- [4] C. Kurtsiefer, S. Mayer, P. Zarda, and H. Weinfurter, *Phys. Rev. Lett.* **85**, 290 (2000).
- [5] A. Hoegele, C. Galland, M. Winger, and A. Imamoglu, *Phys. Rev. Lett.* **100**, 217401 (2008).
- [6] M. S. Hofmann, J. T. Glueckert, J. Noe, C. Bourjau, R. Dehmel, and A. Hoegele, *Nat. Nanotechnol.* **8**, 502 (2013).
- [7] W. Walden-Newman, I. Sarpkaya, and S. Strauf, *Nano Lett.* **12**, 1934 (2012).
- [8] L. Cognet, D. A. Tsyboulski, J.-D. R. Rocha, C. D. Doyle, J. M. Tour, and R. B. Weisman, *Science* **316**, 1465 (2007).
- [9] L. Lueer, S. Hoseinkhani, D. Polli, J. Crochet, T. Hertel, and G. Lanzani, *Nat. Phys.* **5**, 54 (2009).
- [10] S. Moritsubo, T. Murai, T. Shimada, Y. Murakami, S. Chiashi, S. Maruyama, and Y. K. Kato, *Phys. Rev. Lett.* **104**, 247402, 247402 (2010).
- [11] Y.-Z. Ma, L. Valkunas, S. L. Dexheimer, S. M. Bachilo, and G. R. Fleming, *Phys. Rev. Lett.* **94**, 157402 (2005).
- [12] L. Valkunas, Y.-Z. Ma, and G. R. Fleming, *Phys. Rev. B* **73**, 115432 (2006).
- [13] B. Yuma *et al.*, *Phys. Rev. B* **87**, 205412, 205412 (2013).
- [14] Y. Murakami and J. Kono, *Phys. Rev. B* **80**, 035432 (2009).
- [15] Y.-F. Xiao, T. Q. Nhan, M. W. B. Wilson, and J. M. Fraser, *Phys. Rev. Lett.* **104**, 017401 (2010).
- [16] J. J. Crochet, J. G. Duque, J. H. Werner, B. Lounis, L. Cognet, and S. K. Doorn, *Nano Lett.* **12**, 5091 (2012).
- [17] D. M. Harrah and A. K. Swan, *ACS Nano* **5**, 647 (2011).
- [18] T. Hertel, S. Himmelein, T. Ackermann, D. Stich, and J. Crochet, *ACS Nano* **4**, 7161 (2010).
- [19] L. Oudjedi, A. N. G. Parra-Vasquez, A. G. Godin, L. Cognet, and B. Lounis, *J. Phys. Chem. Lett.* **4**, 1460 (2013).

- [20] L. Huang and T. D. Krauss, *Phys. Rev. Lett.* **96**, 057407 (2006).
- [21] U. M. Gösele, *Reaction kinetics and diffusion in condensed matter* (Pergamon Press, New York, 1984), *Progress in Reaction Kintics*, 13 p.^pp. 63-161.
- [22] M. S. Arnold, A. A. Green, J. F. Hulvat, S. I. Stupp, and M. C. Hersam, *Nat. Nanotechnol.* **1**, 60 (2006).
- [23] S. Ghosh, Bachilo, S. M. & Weisman, R. B., *Nat. Nanotechnol.* **5**, 443 (2010).
- [24] P. Nikolaev, M. J. Bronikowski, R. K. Bradley, F. Rohmund, D. T. Colbert, K. A. Smith, and R. E. Smalley, *Chem. Phys. Letts* **313**, 91 (1999).
- [25] G. Wilemski and M. Fixman, *J. Chem. Phys.* **58**, 4009 (1973).
- [26] F. Wang, G. Dukovic, E. Knoesel, L. E. Brus, and T. F. Heinz, *Phys. Rev. B* **70**, 241403(R) (2004).
- [27] T. Koyama, Y. Miyata, H. Kishida, H. Shinohara, and A. Nakamura, *J. Phys. Chem. C* **117**, 1974 (2013).
- [28] D. M. Harrah, J. R. Schneck, A. A. Green, M. C. Hersam, L. D. Ziegler, and A. K. Swan, *ACS Nano* **5**, 9898 (2011).
- [29] S. Berciaud, L. Cognet, and B. Lounis, *Phys. Rev. Lett.* **101**, 077402 (2008).
- [30] L. Oudjedi, Parra-Vasquez, A. N. G., Godin, A. G., Cognet, L. & Lounis, B., *J. Phys. Chem. Lett.* **4**, 1460 (2013).
- [31] F. Wang, Wu, Y., Hybertsen, M. S. & Heinz, T. F., *Phys. Rev. B* **73**, 245424 (2006).
- [32] Y.-S. Park *et al.*, *Phys. Rev. Lett.* **110**, 117401, 117401 (2013).
- [33] G. Nair, J. Zhao, and M. G. Bawendi, *Nano Lett.* **11**, 1136 (2011).
- [34] B. D. Mangum, Y. Ghosh, J. A. Hollingsworth, and H. Htoon, *Opt. Express* **21**, 7419 (2012).
- [35] This prefactor is often neglected under the assumption that  $p_2 = 1$  in the limit of  $\langle N \rangle \rightarrow 0$ . However, for the range of used to determine (Fig. 3c) this prefactor should be included. Details are proved in S10.
- [36] Here, the deviation of experimental points from the theoretically predicted plateau is possibly from tube-to-tube variation in the absorption cross-section values and/or inaccuracies in extracting the and values from PL experiment (Fig. 2).
- [37] S. Ghosh, S. M. Bachilo, R. A. Simonette, K. M. Beckingham, and R. B. Weisman, *Science* **330**, 1656 (2010).

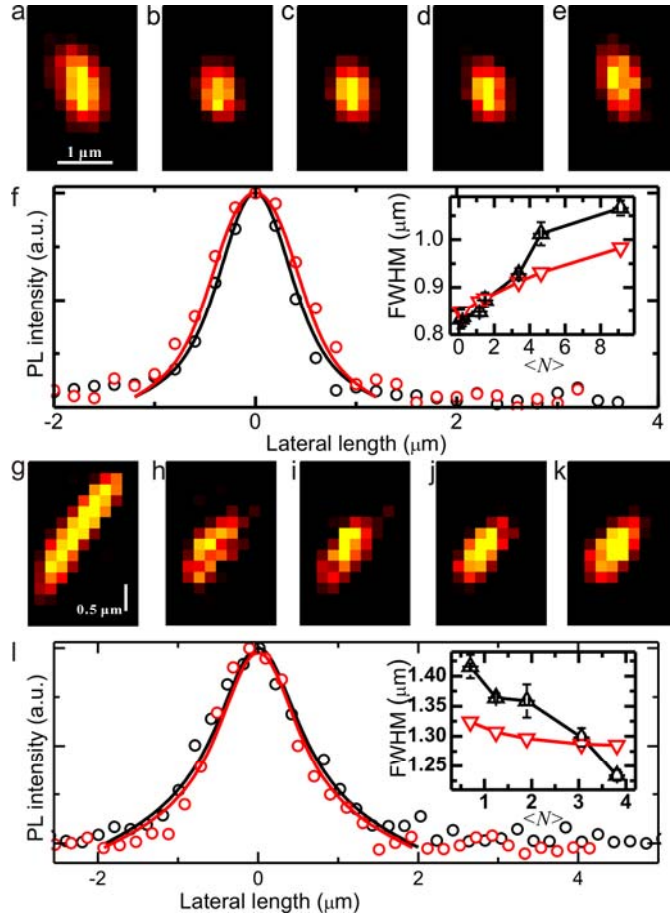


**FIG. 1:** **a, g**, Wide-field PL images of two SWCNTs with lengths of  $\sim 1.2 \mu\text{m}$  (**a**) and  $2.6 \mu\text{m}$  (**g**), respectively. **b-e & h-k**, PL images of the same SWCNTs confocally excited at the center of the tubes. The excitation intensity was increased from  $6.6 \text{ W/cm}^2$  (**b**) to  $535.0 \text{ W/cm}^2$  (**e**), and  $41.2 \text{ W/cm}^2$  (**h**) to  $223.1 \text{ W/cm}^2$  (**k**), respectively. **f, i**, Axial intensity profiles of SWCNT PL images (black circles: **b & h**; red circles: **e & k**) together with the corresponding fitting curves (solid lines). **Insets**, FWHM of measured intensity profiles (black triangles), uncertainty (error-bars) determined from Gaussian fit of the intensity profiles (see S3) and FWHM of calculated (red triangles) PL intensity profiles are plotted as the function of pump fluence given in terms of average number of absorbed photons per laser pulse  $\langle N \rangle$ .

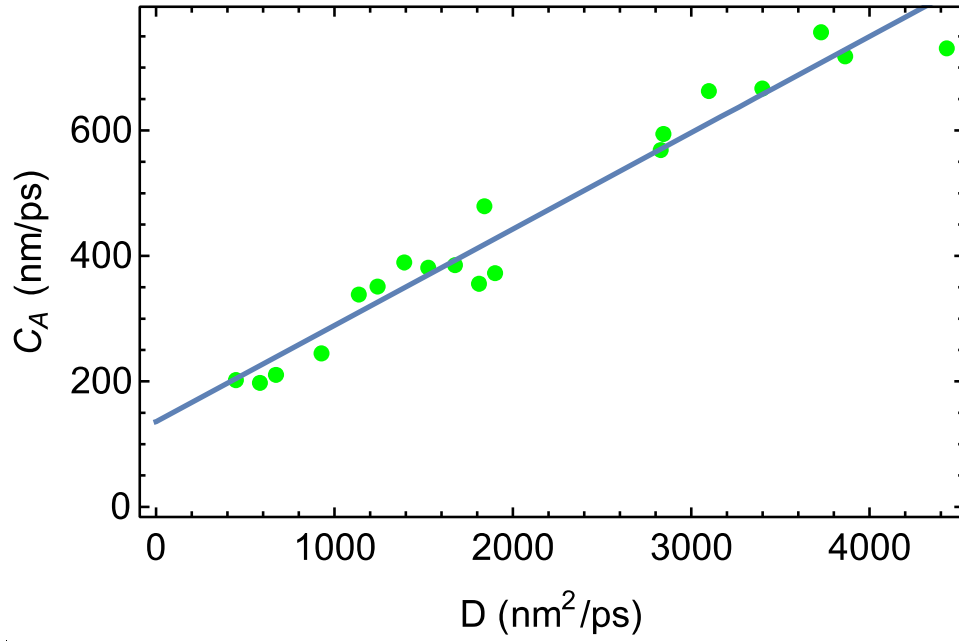


**FIG. 2:** Dots show values of Auger coefficient  $C_A$  and diffusion constant,  $D$ , obtained from global fitting of the intensity profiles of individual SWCNTs using our generalized diffusion model (Eqs. (1) and (2)). Straight line  $C_A \sim D/d_0$  with parameter  $d_0 = 6.5$  nm is a linear fit of the experimental points.

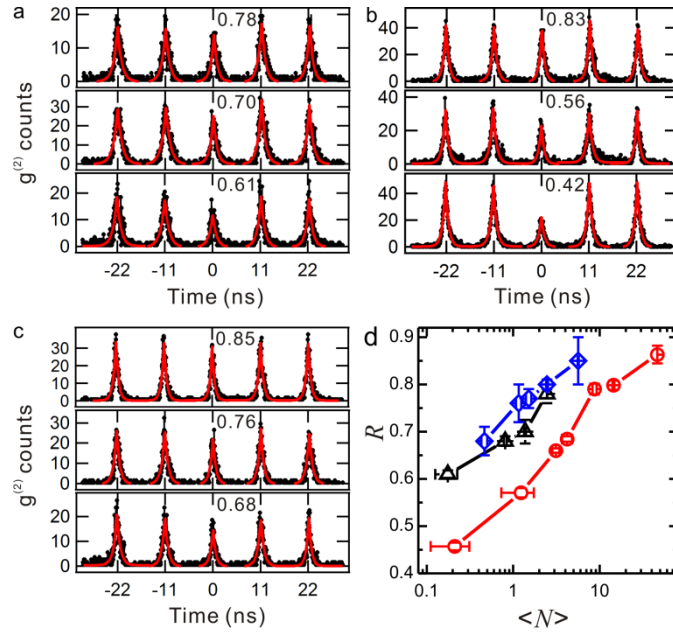


**FIG. 3:** **a-c**, Representative  $g^{(2)}(\tau)$  of three individual SWCNTs with diffusion lengths of 188 nm (a), 336 nm (b), and 525 nm (c) measured at increasing pump fluences (from bottom to top, black dots). Each peak is well fitted by a two-sided exponential function (red curves). The degree of photon-antibunching,  $R$ , is indicated for each curve. **d**,  $R$  of the three individual SWCNTs in part a-c plotted as a function of  $\langle N \rangle$  (black: a; red: b; blue: c).

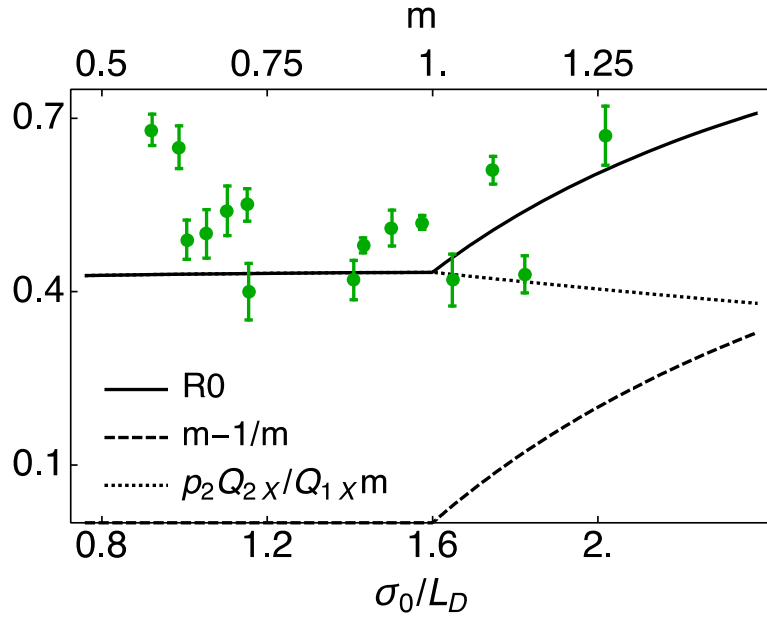


**FIG. 4:** Measured (green circles) and calculated (solid line)  $R_0$  values plotted along with calculated  $p_2 Q_{2X}/(m Q_{1X})$  (dotted line) and  $(m-1)/m$  (dashed line) factors as a function of the ratio  $\sigma_0 / L_D$  and number of independent emitters  $m = \sigma_0 / 1.6 L_D$ .